Original Paper

Adipose-Derived Mesenchymal Stromal Cells Under Hypoxia: Changes in Extracellular Vesicles Secretion and Improvement of Renal Recovery after Ischemic Injury

Federica Collino[a,b,c,d]   Jarlene Alécia Lopes[a,b]   Stephany Corrêa[e]   Eliana Abdelhay[e]
Christina Maeda Takiya[a]   Camila Hübner Costabile Wendt[a]
Kildare Rocha de Miranda[a,b,f]   Adalberto Vieyra[a,b,c,g]   Rafael Soares Lindoso[a,b,c]

[a]Institute of Biophysics Carlos Chagas Filho, Federal University of Rio de Janeiro, Rio de Janeiro, Brazil, [b]National Center for Structural Biology and Bioimaging/CENABIO, Federal University of Rio de Janeiro, Rio de Janeiro, Brazil, [c]National Institute of Science and Technology for Regenerative Medicine-REGENERA, Federal University of Rio de Janeiro, Rio de Janeiro, Brazil, [d]Department of Biomedical Sciences and Paediatric Research Institute "Citta della Speranza", University of Padova, Padova, Italy, [e]National Institute of Cancer, Rio de Janeiro, Brazil, [f]National Institute of Science and Technology of Structural Biology and Bioimaging-INBEB, Federal University of Rio de Janeiro, Rio de Janeiro, Brazil, [g]Program of Translational Biomedicine, Grande Rio University, Duque de Caxias, Brazil

Abstract
Background/Aims: The therapeutic potential of extracellular vesicles (EVs) derived from mesenchymal stromal cells (MSCs) in kidney injury has been largely reported. However, new approaches are necessary to optimize the efficacy in the treatment of renal diseases. MSCs physiologically are under a low O_2 partial pressure (pO_2), and culturing adipose-derived MSCs (ADMSCs) in hypoxia alters their secretory paracrine properties. The aim of this study was to evaluate whether hypoxia preconditioning of ADMSCs alters the properties of secreted EVs to improve renal recovery after ischemia-reperfusion injury (IRI). *Methods:* The supernatants of ADMSCs cultivated under 21% pO_2 (control) or 1% pO_2 (hypoxia) were ultracentrifuged for EVs isolation that were posteriorly characterized by flow cytometry and electron microscopy. The uptake and effects of these EVs were analyzed by using *in vitro* and *in vivo* models. HK-2 renal tubule cell line was submitted do ATP depletion injury model. Proteomic analyses of these cells treated with EVs after injury were performed by nano-UPLC tandem nano-ESI-HDMSE method.

Rafael Soares Lindoso, Ph.D.   Institute of Biophysics Carlos Chagas Filho, Health Sciences Center, Federal University of Rio de Janeiro
and Adalberto Vieyra, Ph.D.   Av. Carlos Chagas Filho, 373 - G1-037 - Ilha do Fundão, Rio de Janeiro - RJ, 21941-902 (Brazil)
Tel. +552139386521; 552139386520, E-Mail lindoso@biof.ufrj.br; avieyra@biof.ufrj.br

For *in vivo* analyses, male Wistar rats were submitted to 45 min bilateral ischemia, followed by renal intracapsular administration of ADMSC-EVs within a 72 h reperfusion period. Histological, immunohistochemical and qRT-PCR analysis of these kidneys were performed to evaluate cell death, inflammation and oxidative stress. Kidney function was evaluated by measuring the blood levels of creatinine and urea. **Results:** The results demonstrate that hypoxia increases the ADMSCs capacity to secrete EVs that trigger different energy supply, antiapoptotic, immunomodulatory, angiogenic and anti-oxidative stress responses in renal tissue compared with EVs secreted in normoxia. Proteomic analyses of renal tubule cells treated with EVs from ADMSCs in normoxia and hypoxia give a specific signature of modulated proteins for each type of EVs, indicating regulation of distinct biological processes. **Conclusion:** In summary, hypoxia potentially offers an interesting strategy to enhance the properties of EVs in the treatment of acute kidney disease.

Introduction

Acute kidney injury (AKI) is defined by a rapid decline in glomerular filtration rate and it presents high mortality rate [1, 2]. Ischemia-reperfusion injury (IRI) is one of the main causes of AKI, characterized by an initial phase of temporary impairment of blood flow and reduction of O_2 supply to the kidney, followed by re-establishment of blood flow and re-oxygenation [3]. The pathophysiology of IRI triggers different pathways associated with inflammation, oxidative stress and cell death, resulting in AKI. Inflammation can be triggered by different types of renal cells, such as injured endothelial and tubular cells that release pro-inflammatory molecules like NF-E2-related factor 2 (Nrf2) and Tumor necrosis factor-alpha (TNF-α). Inflammation is also stimulated by chemotactic cytokines, such as monocyte chemoattractant protein-1 (MCP-1) and macrophage inflammatory protein 2-alpha (MIP-2), which are involved in macrophage and neutrophil recruitment and activation of resident inflammatory cells, culminating in a deleterious process for the kidney [4]. In addition, IRI involves mitochondrial damage and production of reactive oxygen species (ROS). As a compensatory response, renal tubular cells can trigger anti-ROS signaling pathways through the activation of the Nrf2/heme oxygenase-1 (HO-1) axis [5]. However, such response may not be sufficient to maintain the balance between oxidant and antioxidant actions, leading to renal tissue damage and cell death.

Mesenchymal stromal cells (MSCs) display promising curative and preventive therapeutic properties for AKI. More specifically, adipose-derived MSCs (ADMSCs) present immunomodulatory, pro-angiogenic, pro-trophic and anti-apoptotic properties in different organs [6-10]. The mechanism of action of MSCs is mediated mainly by paracrine secretion of growth factors and cytokines, which act on surviving cells of renal tissue, promoting protection against cell death and stimulating proliferation. These processes help to replace the lost cells and, in some cases, promote restoration of renal functioning [10-12].

Extracellular vesicles (EVs) are elements of the paracrine action of MSCs. They comprise a heterogeneous population of vesicles containing part of cytosol of cells from which they derive, surrounded by a lipid bilayer [13]. Several studies of AKI models have reported that administration of EVs derived from bone marrow MSCs (BM-MSCs) gave the same beneficial effects as the administration of BM-MSCs in reducing tubular injury and improvement of renal functioning [14]. EVs derived from ADMSCs also attenuate AKI, reducing fibrosis and preventing the transition from AKI to chronic kidney disease (CKD) [15]. Such effects are mediated by molecules (mRNAs, proteins, lipids) carried by EVs that are horizontally transferred from MSCs to target cells. Proteomic and miRNomic analyses of EVs from BM-MSCs indicated that a different subpopulation of EVs carry specific classes of molecules associated with efficient protection of renal tissue from AKI [16].

Since EVs composition reflects the state of the cell from which they originate, changes in the surrounding environment can alter EVs cargo. Therefore, improvement of renal regenerative potential of EVs may be associated with an *in vitro* cell preconditioning

strategy. Hypoxia has been described to improve the therapeutic potential of ADMSCs [10]. Maintenance of ADMSCs in hypoxic condition has been shown to reduce their apoptosis, to induce their proliferation and to stimulate their pro-angiogenic properties, as well as to improve their homing to the wound environment [17, 18]. In addition, hypoxia alters the secretory paracrine properties of ADMSCs, increasing the release of factors associated with immunomodulation and proliferation needed to support tissue regeneration [19]. Hypoxia also alters ADMSC-EVs cargo and their anti-inflammatory properties [20], i.e. ADMSCs can be "educated" to secrete EVs that account for their different biological effects.

The aim of this study has been to determine whether hypoxia-preconditioning can alter the properties of ADMSC-EVs to improve the support of functional recovery after IRI. We have also investigated the mechanisms involved by analyzing the responses triggered in renal cells after internalization of EVs.

Materials and Methods

Cell Culture

The *in vitro* experiments involved human renal proximal tubule epithelial cells (RPTECs) (HK-2 cells from ATCC, Manassas, VA) cultured in K-SFM medium with 5% fetal calf serum (FCS) (Thermo Scientific, Waltham, MA) (5% CO_2 in air at 37ºC). In other assays, cells were maintained in low-glucose DMEM (Thermo Scientific) in the absence of FCS. Human ADMSCs (Lonza, Basel, Swizerland) were cultured in Adipose-Derived Stem Cell Growth BulletKit™ Medium (Lonza). EVs were isolated from the supernatant of ADMSCs cultured for 72 h in Roswell Park Memorial Institute (RPMI) medium (Thermo Scientific) in normoxic culture conditions (21% O_2; 5% CO_2 at 37ºC) or hypoxic culture conditions (1% O_2; 5% CO_2 at 37ºC) .

ADMSCs characterization

ADMSCs were characterized by fluorescence activated cell sorting (FACS) with a BD FACSCalibur™ instrument (BD Biosciences, San Jose, CA). The antibodies used, phycoerythrin- (PE) or fluorescein-isothiocyanate-conjugated (FITC), were as follows: anti-CD146, anti-CD105, anti-CD90, anti-CD73 and anti-CD44 (BD Biosciences). As control, mouse isotypic IgG conjugated antibodies (BD Biosciences) were used. To test the expression of the exosomal markers CD63, CD81 and CD9, the primary antibodies were obtained from Santa Cruz Biotechnology (Dallas, TX). Labelling with anti-mouse PE and anti-goat FITC secondary antibodies (Thermo Scientific) was carried out as required. ADMSCs expressed CD44, CD73, CD90, CD105, CD63, CD81, did not express CD146, and expression of CD9 was low (Supplementary Fig. 1 - for all supplemental material see www.cellphysiolbiochem.com).

Isolation and characterization of extracellular vesicles (EVs)

The supernatant collected by aspiration from the ADMSC cultures was centrifuged at 300 x g and then at 2, 000 x g for 20 min to remove cells and debris. The supernatants were ultracentrifuged at 100, 000 x g (Optima L-90K ultracentrifuge; Beckman Coulter, Brea, CA) for 2 h at 4°C and the pellets containing ADMSC-EVs were resuspended in RPMI containing 1% DMSO and stored at -80°C in aliquots. EVs derived from ADMSCs cultured in normoxia (EV CTR) and hypoxia (EV HPX) were characterized by flow cytometry using FACSCalibur™ (BD Biosciences). Since the size of EVs is below the detection limit of the flow cytometer, 5 μm latex beads (Aldehyde/Sulfate Latex Beads 4% w/v, Thermo Scientific) were first incubated with EVs for 15 min. The beads surface remained covered with EVs during an incubation period of 30 min with the same antibodies used to characterize ADMSCs. The size and number of isolated EVs were analyzed by NanoSight NS300 instrument (Malvern, United Kingdom) using the Nanoparticle Tracking Analysis (NTA) software 2.1.

AKI in vivo model

All experimental procedures were approved by the Ethics Committee on the Use of Animals in Scientific Experimentation of Federal University of Rio de Janeiro (Protocol A02/16-61-15). Male Wistar rats (200-250 g) were purchased from the Animal Facility of the Institute of Biomedical Sciences of the University of São Paulo, São Paulo, Brazil. Rats were acclimatized for 1 week, maintained under a 12 h light/dark cycle provided with free access to food and water, with a controlled air supply and temperature (22°C).

Cellular Physiology and Biochemistry

Cell Physiol Biochem 2019;52:1463-1483

DOI: 10.33594/000000102
Published online: 18 May 2019

© 2019 The Author(s). Published by
Cell Physiol Biochem Press GmbH&Co. KG

1466

Collino et al.: Hypoxia Alters ADMSC-EVs Renoprotective Effects

Before surgical procedures, the animals were anesthetized by intraperitoneal injection of xylazine (Bayer S.A., São Paulo, Brazil; 5 mg/kg) and ketamine (Cristália, Itapira, Brazil; 50 mg/kg) [16]. The animals were ramdomically distributed into 4 groups: (1) the SHAM group, where rats were given surgical procedures without causing bilateral ischemia; (2) the IRI group, in which the rats were submitted to bilateral renal arterial clamping (45 min) followed by reperfusion with immediate subcapsular injection of PBS, into each kidney after removal of the clamps; (3) the EV CTR group, where the rats were submitted to bilateral renal arterial clamping and received at the beginning of reperfusion – by subcapsular injection into each kidney – 7.5 x 10^8 EVs derived from ADMSCs cultured in normoxia; (4) the EV HPX group, composed by the animals that were submitted to the same surgical procedures followed by subcapsular injection into each kidney of 7.5 x 10^8 EVs derived from ADMSCs cultured in hypoxia. Animals were euthanized 72 h after surgery by intraperitoneal injection of a high dose of xylazine (30 mg/kg) and ketamine (200 mg/kg). Blood samples were collected in tubes previously treated with 1 mM Na_2EDTA solution. The kidneys were removed and processed for histological and molecular analysis. Blood urea nitrogen (BUN) and creatinine were measured by using the respective kits for colorimetric assays [21, 22], following the manufacturer's protocols (Bioclin, Belo Horizonte, Brazil).

Histological score of tubular lesions
The kidneys were fixed, dehydrated, and embedded in paraffin as previously described [23]. Cortical slices (5 μm) were stained with hematoxylin and eosin (Sigma-Aldrich) and observed under light microscopy. Images from 30-35 fields from each group were taken randomly, and proximal tubular injury was analyzed for the following parameters: cell detachment, brush border integrity, presence of hyaline casts and nuclear alterations. The interstitial compartment was analyzed for enlargement, inflammation and the presence of connective tissue fibers. An injury score was assigned on a 3-point scale. The score and the parameters were as follows: 0 – no alterations; 0.5 – mild alterations affecting 10% or fewer tubules; 1 – alterations affecting 25% tubules; 1.5 – alterations affecting 45% tubules; 2.0 – alterations affecting 60% tubules; 2.5 – alterations affecting 75% tubules; and 3 – alterations in more than 75% of tubules (maximum interstitial injury degree: 9; maximum tubule injury degree: 12). The injury score was given by the sum of interstitial and tubule damage.

Immunohistochemistry
Immunohistochemistry involved an immunoenzymatic technique applied to 5 μm paraffin sections, which underwent heat-induced antigen retrieval by microwave in 0.01 M Na-citrate buffer (pH 6.0). For ED-1 staining, incubation with 0.1% Trypsin solution was included in the labelling protocol. Slides were then incubated overnight at 4°C in a humid chamber with the primary antibodies. Binding was detected by incubation with Rat Simple Stain anti-mouse secondary antibody (Nichirei Bioscience, Chuo-ku, Tokyo, Japan) for 1 hour at room temperature. Peroxidase was detected with 3, 3'-diaminobenzidine (Liquid DAB, Agilent Technologies, Santa Clara, CA) as chromogen, and the slices counterstained with hematoxylin. Antibodies against PCNA (Agilent Technologies), ED-1/CD68 (Bio-Rad, Hercules, CA), Nrf2 phospho S40 (Abcam, Cambridge, United Kingdom) and HO-1 (Abcam) were used. Sections were incubated with isotype specific immunoglobulins as negative controls.

Histomorphometry analyses used a computer-assisted image analysis system (Nikon Eclipse E-800 microscope connected to a computer by a digital camera Evolution, Media Cybernetics Inc., Tallahassee, FL) coupled to the software Q-Capture 2.95.0 (Silicon Graphic Inc.). Fifteen high quality photomicrographs (2048 × 1536 pixel) were captured from non-overlapping renal cortical areas with a 20x or 40x objective lens. Measurements of HO-1 expression in renal tubule cells are given as a percentage of tissue surface area in renal cortical tubules measured by ImageJ software. PCNA, and ED-1 were determined by the number of positive cells in each field. Nrf2 was determined by number of cells with positive nuclei in each field.

Electron microscopy
Renal tissue samples and ADMSC were washed in Dulbecco's PBS (pH 7.2), fixed in 2.5% glutaraldehyde with 4% freshly prepared formaldehyde in 0.1 M cacodylate buffer (pH 7.2) for 24 hours. Following a wash in cacodylate buffer 0.1 M, the samples were post-fixed in 1% osmium tetroxide plus 0.8% potassium ferrocyanide in 0.1 M cacodylate buffer for 40 minutes, dehydrated in acetone and embedded in epoxide resin. Ultrathin sections (70 nm) were cut and stained for 20 minutes in 5% aqueous uranyl acetate and for

Cellular Physiology and Biochemistry

Cell Physiol Biochem 2019;52:1463-1483

DOI: 10.33594/000000102
Published online: 18 May 2019

© 2019 The Author(s). Published by
Cell Physiol Biochem Press GmbH&Co. KG

1467

Collino et al.: Hypoxia Alters ADMSC-EVs Renoprotective Effects

5 minutes in lead citrate. A Tecnai-Spirit transmission electron microscope (Thermo Scientific) operating at 120 kV was used to take images.

EVs were isolated as described above and 10 μl of a suspension of vesicles in PBS were adhered onto glow-discharged formvar-coated copper grids 300 mesh (EMS, Hatfield, PA) for 10 minutes. Excess solution was removed using Whatman no 1 filter paper (Thermo Scientific). Grids were subsequently negatively stained with 1% aurothioglucose (USP) in water for 30 seconds, dried with a filter paper and examined in the electron microscope.

Western blotting

Expression of Bcl-2 associated X (Bax) and B-cell lymphoma 2 (Bcl-2) were measured by Western blotting. The antibodies were purchased from Cell Signaling Technology (Leiden, Netherlands), with β-actin used as loading control (Sigma-Aldrich). The secondary antibodies were goat anti-rabbit and anti-mouse IgG-HRP (Santa Cruz Biotechnology). Proteins on Western blots were detected by chemiluminescence using the ECL™ system (GE Healthcare) coupled to a ChemiDoc XRS+(Bio-Rad). Quantification of Western blots relied on ImageJ software.

ATP depletion in vitro injury model and intracellular ATP measurement

RPTECs were incubated for 30 min with Hank's Balanced Salt Solution (Thermo Scientific) containing 1 μM antimycin A (Sigma-Aldrich) and 10 mM 2-deoxyglucose [24]. The cells were washed with PBS and incubated in low-glucose DMEM for 24 h at 37°C under air with 5% CO_2 in the absence or presence of ADMSC-EVs (3 x 10^3 vesicles/renal cell). RPTEC intracellular ATP was measured using an Adenosine 5′-triphosphate (ATP) Bioluminescent Assay Kit for ATP (Sigma-Aldrich) using a GloMax®-Multi Microplate Reader (Promega, Madison, WI). The results give the level of intracellular ATP under each condition with respect to SHAM control.

RNA isolation and quantitative real-time polymerase chain reaction (qRT-PCR)

mirVana RNA isolation kit (Thermo Scientific) was used for RNA extraction from renal tissue, RNA being measured spectrophotometrically (Nanodrop ND-1000, Thermo Scientific). mRNA expression was assessed using a High Capacity cDNA Reverse Transcription Kit (Applied Biosystems) and Power SYBR® Green PCR Master Mix (Applied Biosystems). Negative cDNA controls (no cDNA) were cycled in parallel with each run. qRT-PCR was done with a ViiA™ 7 Real-Time PCR System (Applied Biosystems). All the sequence-specific oligonucleotide primers were obtained from Eurofins Genomics (Ebersberg, Germany). See Supplementary Table 1 for primers sequences.

EVs labeling and internalization by renal cells

The EVs labelling protocol was adapted from [25]. Briefly, isolated EVs were labelled with 1 μM Vybrant Cell Tracers DiI (for *in vitro* experiments) or 1 μM Vybrant Cell Tracers DiD (for *in vivo* experiments) (Molecular Probes) in RPMI without serum during the ultracentrifugation procedure at 100, 000 g for 2 hours at 4°C. They were washed twice by ultracentrifugation in PBS and resuspended in 50 μl PBS. As a control for the labelling, 1 μM Vybrant Cell Tracers DiI or DiD was also ultracentrifuged in RPMI in the absence of EVs and washed twice with PBS. Although no pellet was obtained, 50 μl PBS was added to the tube and collected for subsequent incubation with RPTECs.

To analyze EVs uptake *in vitro*, RPTECs cells were plated on coverslips treated with attachment factor (Thermo Scientific). The cells were subjected to ATP depletion injury (30 min) and then incubated for 24 hours with labelled EV CTR, EV HPX or PBS ultracentrifuged with Vybrant DiI (2 hours). The cells were washed with PBS and fixed with 4% paraformaldehyde. Nuclei were stained with 4′,6-diamidino-2-phenylindole (DAPI). The images were with an EVOS FL Cell Imaging System (Thermo Scientific).

For the *in vivo* model, Vybrant DiD-stained EVs were injected after 45 minutes of bilateral ischemia, as described in the "AKI *in vivo* model" section. After 24 hours the animals were euthanized and the kidneys removed for measurement of fluorescence using IVIS Lumina System (Xenogen Corp., Alameda, CA).

Cellular Physiology and Biochemistry

Cell Physiol Biochem 2019;52:1463-1483

DOI: 10.33594/000000102
Published online: 18 May 2019

© 2019 The Author(s). Published by
Cell Physiol Biochem Press GmbH&Co. KG

1468

Collino et al.: Hypoxia Alters ADMSC-EVs Renoprotective Effects

Angiogenesis assay

Human umbilical vein endothelial cells (HUVECs) were kindly donated by Dr. Giovanni Camussi. HUVECs (2 x 10^4 cells) were plated in 24-well plates coated with growth-factor depleted Matrigel® (Corning) and cultured in the absence or presence of ADMSC-EVs (EV CTR or EV HPX) for 24 hours in DMEM without FCS. As a positive control, cells were cultured in Endothelial Complete Medium (EBM-2, Lonza). The EVs angiogenic potential was determined by the number of vascular-like structures formed by endothelial cells per field [26].

Label-free protein quantitation via mass spectrometry analyses

To obtain protein extracts for proteomic analysis, RPTECs from all conditions (CTR, INJ, INJ-EV CTR and INJ-EV HPX) were resuspended in 200 μl cold lysis solution containing 50 mM Tris-HCl (pH 7.5), 5 mM EDTA, 10 mM EGTA, 50 mM NaF, 20 mM KCl and 250 mM NaCl, supplemented with 1 μl protease inhibitor cocktail (GE Healthcare, Life Sciences, Piscataway, NJ). The suspension was frozen and thawed 3 times in liquid N2 and incubated on ice for 30 minutes. The lysates were centrifuged at 12, 000g for 30 minutes, and the supernatants were collected for storage at -80°C. Proteomic analysis was conducted with pooled triplicates for each condition. Protein quantification was achieved using the Bradford assay, and the samples were concentrated in a 3 kDa ultra-filtration device (Millipore, Burlington, MA) and exchanged with 50 mM NH4HCO3. A total of 200 μg protein was used for tryptic digestion, as previously reported [27]. The proteomic approach applied here was the nano-Ultra Performance Liquid Chromatography (nano-UPLC) tandem nano-ESI-HDMSE method for qualitative and quantitative experiments. A nanoACQUITY UPLC system (Waters, Waters, United Kingdom) was employed, as previously reported by [28]. The LC/MSMS approach generated high-quality data for proteins identification and quantification. The False Discovery Rate (FDR) percentage for both peptide and protein level were <1% (0.6 for all conditions), with an average of 6 peptides per protein identification.

Database searching and protein quantification used the PLGS Expression E tool algorithm. Identified proteins were organized into a statistically significant list corresponding to increased and decreased regulation ratios between the assayed cells (CTR, INJ+EV CTR or INJ+EV HPX conditions) compared with INJ condition. In silico analysis for system biology with network interactions and biological processes used Metacore™ software (Clarivate Analytics, Philadelphia, PA).

Statistical analysis

Statistical analyses used the Student t-test or the one-way analysis of variance (ANOVA) test with Tukey's post-test. Statistical significance was set at $P < 0.05$. Data were analyzed using the GraphPad Prism 5.0 program. The data are expressed as mean ± SEM.

Results

Hypoxia modulates the secretion of EVs by ADMSCs

Electron microscopy images (Fig. 1) showed the presence of structures resembling multivesicular bodies, exosomes and microvesicles secreted by ADMSCs under normoxia (Fig. 1A-1D) and hypoxia (Fig. 1G-1J). At the surface of ADMSCs under hypoxia, the presence of a higher number of vesicles budding from the plasma membrane could be seen (Fig. 1I), indicating a possible increase in EVs secretion. Electron microscopy images were also taken of EVs isolated by ultracentrifugation from the ADMSCs supernatant. In both conditions, EVs were of a size that comprises both exosomes and microvesicles (Fig. 1E, 1K). High magnification images show the bilipid membrane delimiting the secreted ADMSC-EVs (Fig. 1F, 1L).

Characterization of isolated EVs by NanoSight (Malvern, Malvern, United Kingdom) confirmed in both conditions the presence of a heterogeneous EVs population containing exosomes and microvesicles, but not apoptotic bodies (Fig. 1M, 1N). Quantification of EVs showed a 2-fold increase in the number of EVs secreted by ADMSCs under hypoxia (CTR: 5487 ± 519 EVs/cell; HPX: 9181 ± 872 EVs/cell) (Fig. 1O). The mean size of EV CTR was 156.4 ± 10.5 nm and EV HPX was 138.0 ± 11.2 nm, indicating a small, but not significant,
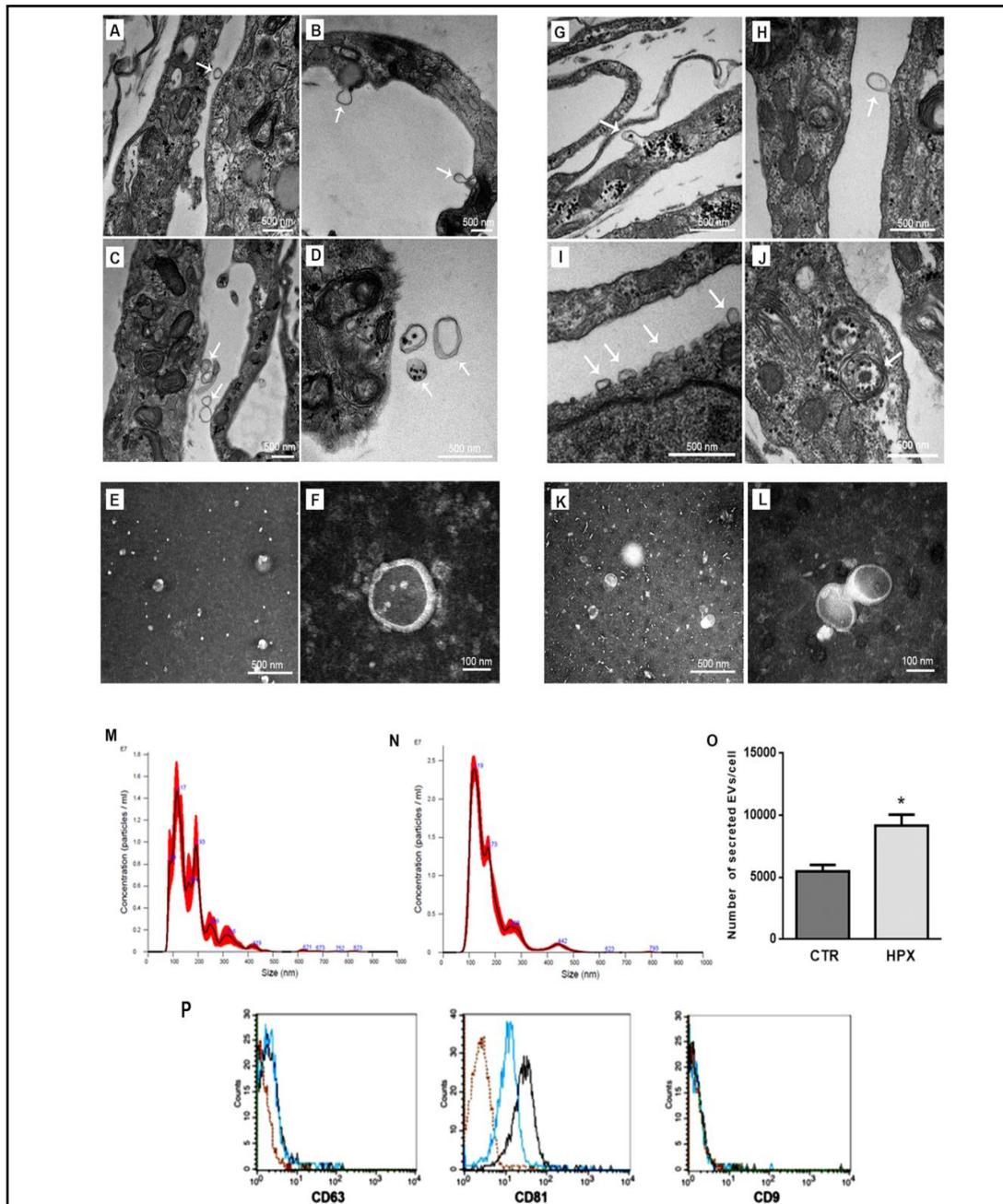
Collino et al.: Hypoxia Alters ADMSC-EVs Renoprotective Effects

Fig. 1. Modulation of ADMSC-EVs secretion by hypoxia. Electron microscopy images of ADMSCs cultured for 72 h in normoxia and the presence of vesicular structures indicated by white arrows, scale bars = 500 nm (A-D). Images of EVs isolated from ADMSCs cultured in normoxia, scale bar in E = 500 nm, scale bar in F = 100 nm (E, F). Images of ADMSCs cultured for 72 h in hypoxia and the presence of vesicular structures indicated by white arrows, scale bars = 500 nm (G-J). Images of EVs isolated from ADMSCs cultured in hypoxia, scale bar in K = 500 nm, scale bar in L = 100 nm (K, L). Representative Nanosight analysis of size distribution of EV CTR (M) and EV HPX (N) isolated from ADMSCs supernatant. Relation between the number of EVs isolated from supernatant and the number of ADMSCs in culture. Data represent mean ± SEM (n = 8). (*, P<0.05, assessed by the t-test) (O). Representative micrograph of EVs characterization by flow cytometry showing positivity for exosome markers CD63 and CD81, but not CD9. The lines indicate the fluorescent intensity for each marker: black line indicates EV CTR, blue line indicates EV HPX and red line indicates EVs incubated with secondary IgG, as negative control (P). Abbreviations: EV, extracellular vesicles; CTR, control; HPX, hypoxia.

1470

Collino et al.: Hypoxia Alters ADMSC-EVs Renoprotective Effects

difference in size between the two conditions. FACS analysis of both EVs showed the presence of classical MSC markers: CD73, CD90 and CD105 (Supplementary Fig. 2). EV CTR and EV HPX also expressed the exosomal markers CD63 and CD81, but not CD9 (Fig. 1P).

EVs internalization and activity in RPTECs

We initially focused on the role of ADMSC-EVs in cultured RPTECs, due to their susceptibility in *in vitro* injury model that mimics IRI in terms of O_2 availability and elevated CO_2 partial pressure (Fig. 2). RPTECs submitted to depletion of ATP showed, after 24 h, similarly internalized EV CTR and EV HPX (Fig. 2A).

The renoprotective effect of ADMSC-EVs was assessed by measuring cell death rate (annexin V/PI staining). The ATP depletion model resulted in cell death by necrosis (Annexin V+/PI+), although some cells were apoptotic (Annexin V+/PI-) after 24 h (Fig. 2B). In renal cells with ATP depletion injury (INJ), there was an increase in cell death compared to the control group (CTR: 6.3 ± 0.9%; INJ: 24.3 ± 1.0%). Both EVs reduced cell death, but EV HPX showed a more accentuated protective effect (INJ+EV CTR: 17.2 ± 1.5%; EV HPX: 12.2 ± 1.0%) (Fig. 2C).
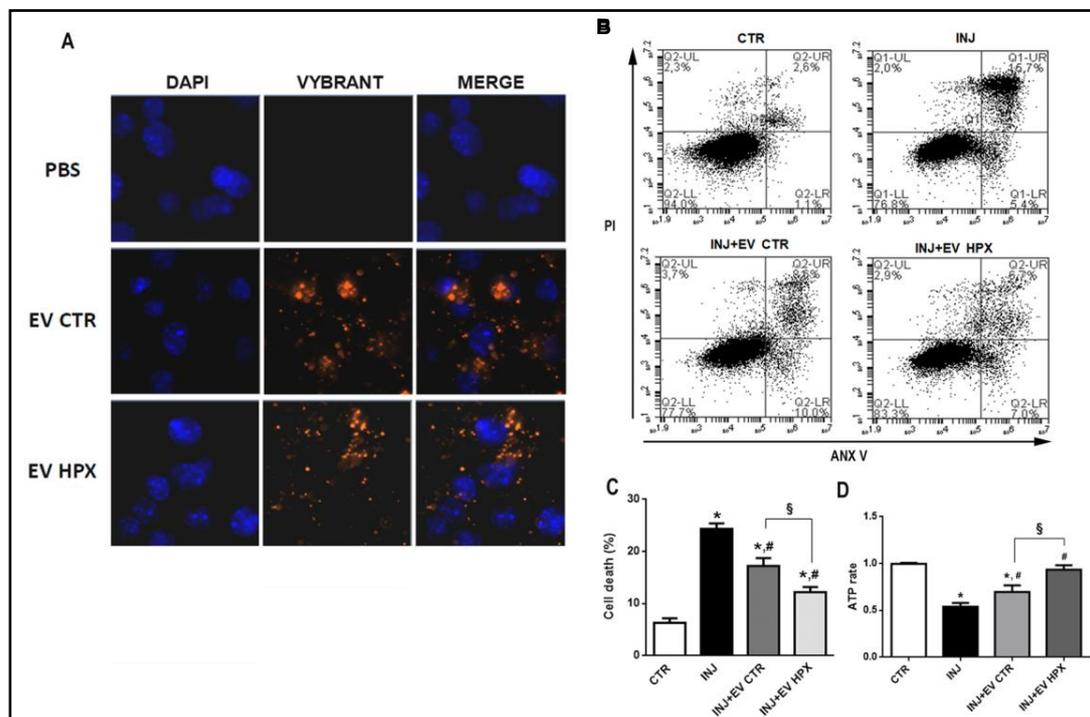

Fig. 2. EV CTR and EV HPX uptake by RPTECs and their protective effect after ATP depletion injury in an *in vitro* model. Representative fluorescent images of RPTECs incubated for 24 h after injury with EV CTR or EV HPX previously stained with Vybrant DiI (red fluorescence). Renal cell nuclei were stained with DAPI (blue fluorescence). PBS condition indicates the staining protocol in the absence of vesicles in order to exclude the non-specific signal given by Vybrant DiI aggregates (A). Flow cytometry analyses of renal cells marked for ANX V/PI under the different experimental conditions: CTR (cells not ATP depleted), INJ (cells submitted to ATP depletion), INJ+EV CTR (cells ATP depleted followed by 24 h incubation with EV CTR) and INJ+EV HPX (cells ATP depleted followed by 24 h incubation with EV HPX) (B). Quantification of flow cytometry analysis to determine the rate of cell death of renal cells in all groups (n = 6) (C). Levels of intracellular ATP (ATP rate with respect to SHAM) of renal tubule cells under the 4 experimental conditions (n = 7) (D). Data represent mean ± SEM. (* indicates statistical difference to SHAM group; # indicates statistical difference to IRI group, § indicates statistical difference to IRI+EV CTR group, P<0.05 assessed by one-way ANOVA followed by Tukey's test). Abbreviations: RPTECs: renal tubule epithelial cells; EV extracellular vesicles; CTR, control; HPX, hypoxia; INJ, injury; PI, propidium iodide; ANX V, annexin V, DAPI, 4',6-Diamidino-2-Phenylindole; PBS, phosphate buffered saline.

Since this injury model reduces intracellular ATP, we determined whether the protective effect of EVs were associated with the maintenance of ATP levels (Fig. 2D). RPTECs maintained for 24 h in culture after incubation with antimycin A still had reduced intracellular ATP (ratio: 0.54 ± 0.01) in comparison to the CTR group (0.99 ± 0.01). Incubation with EV CTR gave partial recovery of ATP levels (ratio INJ+EV CTR: 0.70 ± 0.03), whereas incubation with EV HPX resulted in a full recovery of intracellular ATP levels (ratio INJ+EV HPX: 0.93 ± 0.02).

ADMSC-EVs induced angiogenesis in vitro

We also evaluated the angiogenic capacity of ADMSC-EVs following the formation HUVEC capillary-like structures (Fig. 3). As anticipated, HUVEC cultured in basal DMEM medium produced few capillary-like structures (5.5 ± 1.2 structures/field) (Fig. 3B, 3E) compared to those cultured in endothelial basal medium (48.1 ± 3.5 structures/field) (Fig. 3A, 3E). Incubation for 24 h with EV CTR significantly increased the formation of capillary-like structures (14.9 ± 1.6 structures/field) (Fig. 3C, 3E), and incubation with EV HPX induced even greater accentuation of angiogenesis (21.9 ± 1.9 structures/field) (Fig. 3D, 3E).

Proteomic analysis shows different signatures triggered by EV CTR and EV HPX in renal cells

To understand the direct effects of EVs and the responses triggered inside renal cells, proteomic analysis of RPTECs cultured in all *in vitro* conditions (CTR, INJ, INJ+EV CTR, INJ+EV HPX) were performed. Our observed groups of proteins differentially expressed were associated with injury and recovery processes (Fig. 4, Supplementary Tables 2-4). The Venn diagram shows the number of proteins differentially expressed in each condition with respect to INJ. CTR indicated 254 proteins, INJ+EV CTR 210 proteins and INJ+EV HPX 151 proteins, with an altered expression with respect to INJ (Fig. 4A, 4B). Fifty-nine proteins had the same pattern of expression in both EVs treatment (5 upregulated and 54 downregulated with respect to INJ); 151 proteins (117 upregulated and 34 downregulated) were modulated

Fig. 3. Hypoxia increases angiogenic potential of ADMSC-EVs. Representative photomicrographs of HUVEC under different culture conditions for 24 h: EBM (HUVEC cultured in complete EBM medium) (A), DMEM NO FCS (HUVEC cultured in DMEM depleted of FCS) (B), EV CTR (HUVEC cultured in DMEM depleted of FCS, in the presence of EV CTR) (C) and EV HPX (HUVEC cultured in DMEM depleted of FCS, in the presence of EV HPX) (D). Quantification of the number of capillary-like structures/fields observed under each condition (n = 3) (E). Data represent mean ± SEM. (* indicates statistical difference to SHAM group; # indicates statistical difference to IRI group, § indicates statistical difference to IRI+EV CTR group, P<0.05 assessed by one-way ANOVA followed by Tukey's test). Abbreviation: HUVEC, human umbilical vein endothelial cells; EBM, Endothelium Basal Medium; DMEM, Dulbecco's Modified Eagle Medium; FCS, fetal calf serum; EV, extracellular vesicles, CTR, control; HPX, hypoxia.
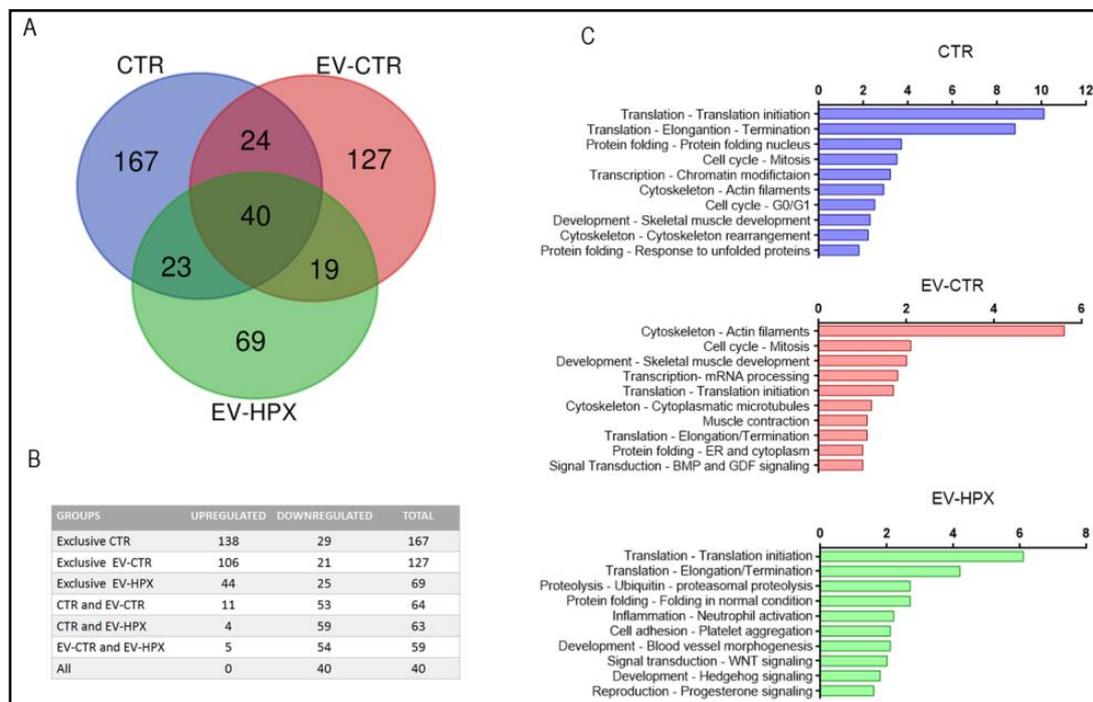
Collino et al.: Hypoxia Alters ADMSC-EVs Renoprotective Effects
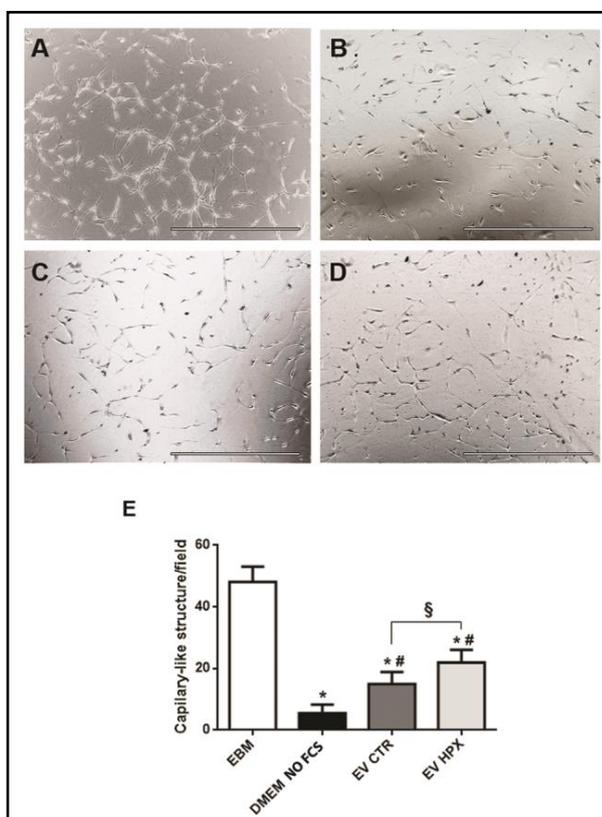
Fig. 4. EV CTR and EV HPX trigger different biological process inside renal tubule cells submitted to ATP depletion injury. Venn diagram from proteomic analyses shows the number of identified proteins differentially expressed in renal cells in all experimental groups under injury due to ATP depletion (INJ), where CTR indicates the condition in which cells were not ATP depleted, EV CTR indicates ATP depleted cells followed by 24 h incubation with EV CTR, and EV HPX indicates ATP depleted cells followed by 24 h incubation with EV HPX (A). The table shows the number of proteins upregulated and downregulated under all experimental conditions in respect to the injury condition (INJ) (B). Identification, by METACORE analysis, of biological processes associated with the proteins differentially expressed in the 3 different groups (CTR, EV CTR, EV HPX) in respect to the injury condition (C). Abbreviations: EV, extracellular vesicles, CTR, control; HPX, hypoxia.

by EV CTR, but not by EV HPX. EV HPX incubation led to the modulation of 92 proteins (48 upregulated and 44 downregulated) that were not modified by EV CTR (Fig. 4B). Functional analysis of data showed modulation of important biological processes associated with protection and recovery of renal injury (Fig. 4C).

The most relevant biological processes related with the proteins modulated by EV CTR treatment are those associated with cytoskeleton reorganization, cell cycle regulation, transcriptional and translational regulation, protein folding and the signal transduction processes linked to Bone Morphogenetic Protein (BMP) and Growth Differentiation Factor (GDF). In common with EV CTR, EV HPX modulate processes related to protein folding and transcriptional and translational regulation, and, selectively, several other processes including proteolysis regulation, inflammation, cell adhesion, development and signal transduction (e.g. Wingless/Integrated, Wnt signaling). Finally, we analyzed the biological processes altered after INJ compared with CTR condition. Changes were associated with transcriptional and translational regulation, protein folding, cell cycle regulation, development and cytoskeleton reorganization.

ADMSC-EVs promote recovery of renal function after IRI

In order to evaluate if the enhanced protective effects of EV HPX observed *in vitro* would also be observed *in vivo*, we first analyzed the uptake of both EVs by renal cells *in vivo* (Fig. 5). Tracking of Vybrant DiD-stained EVs showed the presence of EV CTR and EV HPX in the kidney for 24 h after subcapsular injection (Fig. 5A). Functioning of the kidney was evaluated,
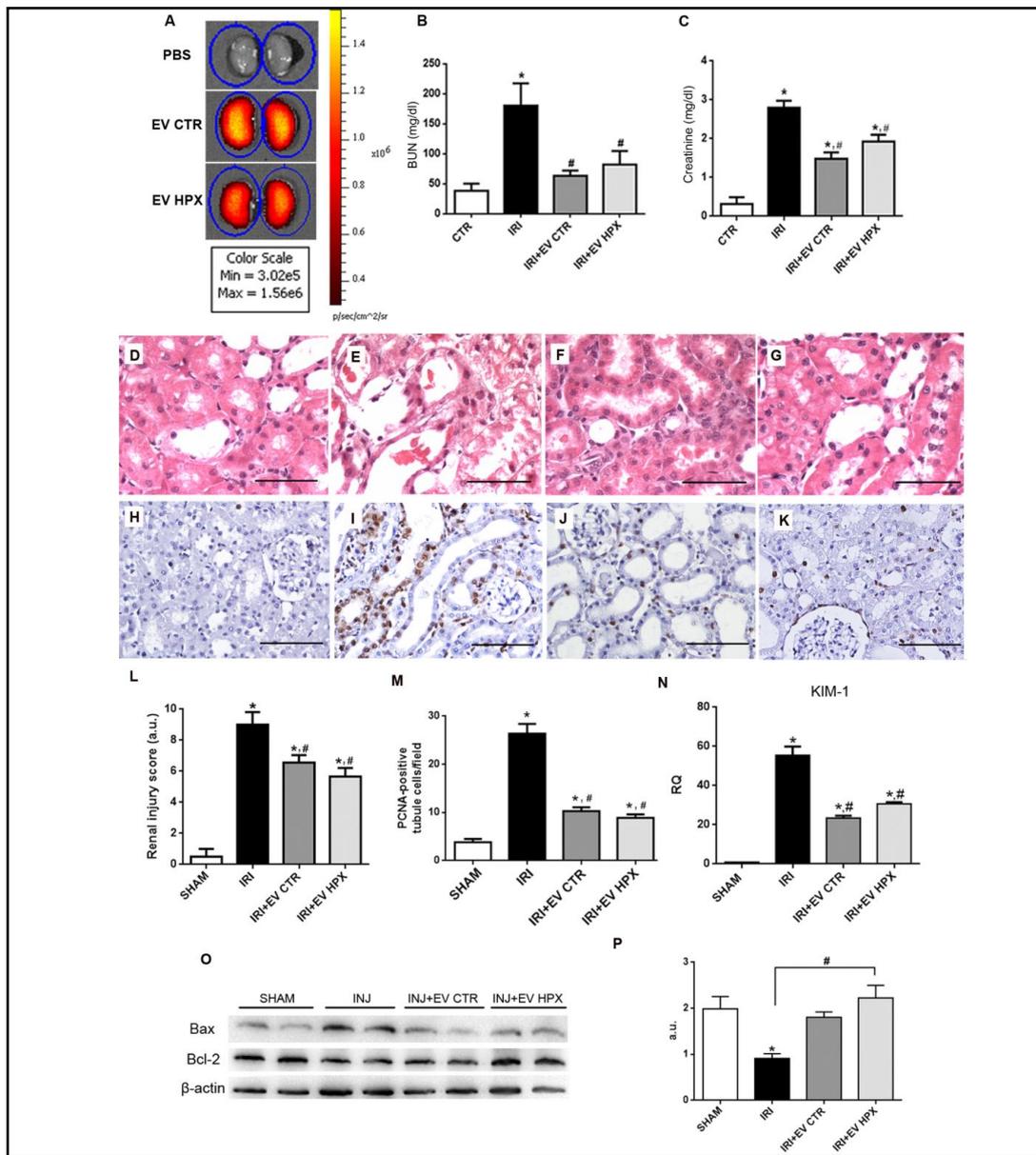
Cellular Physiology and Biochemistry

Cell Physiol Biochem 2019;52:1463-1483

DOI: 10.33594/000000102
Published online: 18 May 2019

© 2019 The Author(s). Published by
Cell Physiol Biochem Press GmbH&Co. KG

1473

Collino et al.: Hypoxia Alters ADMSC-EVs Renoprotective Effects

Fig. 5. EVs localization and their renoprotective effects. Fluorescent detection of administered EVs stained with Vybrant DiD. Color scale bar indicates the fluorescence intensity associated with EVs presence. PBS indicates the staining protocol without EVs to exclude possible nonspecific dye signal (A). Measurement of blood BUN (B) and creatinine (C) (n = 8) levels in IRI treated and SHAM animals. Kidney cortical slices stained with H/E: SHAM (D), IRI (E), IRI+EV CTR (F) and IRI+EV HPX (G) (scale bar = 50 μm). Representative photomicrographs of immunohistochemistry for PCNA: SHAM (H), IRI (I), IRI+EV CTR (J) and IRI+EV HPX (K) (scale bar = 100 μm). Histological score of tubular lesions (SHAM, n (kidneys) = 10; IRI, IRI+EV CTR, IRI+EV HPX, n (kidneys) = 12) (L). Number of PCNA-positive cells/field from immunohistochemistry (n = 10 fields for 4 kidneys) (M). KIM-1 mRNA levels in renal tissue expressed as RQ in respect to SHAM group (n = 5) (N). Representative western blot of Bax/Bcl-2 expression in renal tissue (O) and quantification of the ratio Bcl-2/Bax (n = 4) (P). Data represent mean ± SEM. (* indicates statistical difference to SHAM group; # indicates statistical difference to IRI group, P<0.05 assessed by one-way ANOVA followed by Tukey's test). Abbreviations: H/E, hematoxylin/eosin; PBS, phosphate buffered saline; BUN, blood urea nitrogen; EV extracellular vesicles; SHAM, false operate; CTR, control; HPX, hypoxia; IRI, ischemia-reperfusion injury; KIM-1, Kidney Injury Molecule-1; Bcl-2, B-cell lymphoma 2; Bax, Bcl-2 associated X, β-actin, beta-actin; PCNA, proliferating cell nuclear antigen; a.u., arbitrary units; RQ, relative quantification.

Cellular Physiology and Biochemistry

Cell Physiol Biochem 2019;52:1463-1483

DOI: 10.33594/000000102
Published online: 18 May 2019

© 2019 The Author(s). Published by
Cell Physiol Biochem Press GmbH&Co. KG

1474

Collino et al.: Hypoxia Alters ADMSC-EVs Renoprotective Effects

72 h after ischemic insult and EVs subcapsular injection, by measuring BUN and creatinine levels in blood (Fig. 5B, 5C, respectively). In the IRI animals, blood creatinine (2.8 ± 0.1 mg/dl) and BUN levels (180.6 ± 36.9 mg/dl) increased, indicating reduced glomerular filtration rate (GFR). Administration of EV CTR and EV HPX partially (and significantly) protected the kidneys function, as seen by a reduction in the creatinine levels (EV CTR: 1.5 ± 0.1 mg/dl; EV HPX: 1.9 ± 0.1 mg/dl), SHAM animals having normal levels of creatinine (0.3 ± 0.1 mg/dl). Groups given EVs treatment were not statistical different from each other (P = 0.09). In EV CTR and EV HPX rats, there was also a strong reversion of BUN levels with respect to the IRI animals (55.5 ± 11.1 and 82.1 ± 26.6 mg/dl, respectively), relative those in the SHAM group (40.9 ± 2.3 mg/dl). In the BUN levels, no significant difference was seen between the groups given EVs treatment (P = 0.08).

Renoprotective effects of ADMSC-EVs in IRI

Tissue damage was first evaluated by examining histological images of cortical kidney sections (Fig. 5D-5G, 5L). In animals submitted to IRI, indicators of tissue damage included loss of brush border, epithelial cell detachment, the presence of hyaline casts and nuclear alterations, resulting in a score of 9.0 ± 0.8 (Fig. 5E, 5L). EV CTR treatment significantly reduced the intensity and the area of tissue damage, giving a score of 6.6 ± 0.5 (Fig. 5F, 5L). With an equivalent number of EV HPX treatment, similar effects gave a score of 5.7 ± 0.5 (Fig. 5G, 5L).

The proliferation rate of RPTECs was analyzed by quantification of PCNA-positive cells (Fig. 5H-5K, 5M). As expected after 72 h of ischemia, the cortical region of the kidneys of IRI group had a robust increase in the number of proliferating cells (26.4 ± 0.7 cells/field), indicating an attempt to recover from the injury (Fig. 5I). Kidneys treated with EV CTR or with EV HPX had reduced levels of PCNA-positive cells (10.3 ± 0.4 and 8.9 ± 0.3 cells/field, respectively) (Fig. 5J, 5K). Although the proliferation rates were significantly higher than in the SHAM group (3.9 ± 0.3 cells/field), both EVs treatments substantially reduced PCNA-positive cells compared to IRI group. These results suggest that the decrease in the proliferative response is due to a reduction in tissue damage due to EVs administration.

The protective role of EVs was also followed by changes in KIM-1 expression (Fig. 5N), a specific and sensitive biomarker of renal injury [29]. Kidneys of IRI treated animals presented significant change in the expression of this marker (55-fold increase with respect to SHAM). Both EV CTR and EV HPX partially, but again significantly, abrogated KIM-1 upregulation (23- and 30-fold increase in relation to the SHAM controls, respectively). No significant difference was found between EV CTR and EV HPX treatment (P = 0.14).

EV HPX treatment shifts the Bcl-2/Bax pattern from cell death to cell survival

Bcl-2 (anti-apoptotic) and Bax (pro-apoptotic) are key proteins associated with mitochondrial damage and cell death. Animals submitted to IRI presented decreased Bcl-2 protein levels in relation to Bax, indicating that cells were moving toward a death program. This was partially reversed when EV CTR were administered, but no significantly (P = 0.1) from the IRI group. Treatment with EV HPX, however, led to a total re-establishment of the ratio Bcl-2/Bax to that in the SHAM group (Fig. 5O, 5P).

EV CTR and EV HPX trigger different anti-oxidative stress responses

Mitochondrial morphology, seen by electron microscopy (Fig. 6), showed altered features in ischemic kidneys, with intense vacuolization of the matrix, a typical ultrastructural characteristic of damage. Mitochondria from ischemic kidneys treated with EV CTR or EV HPX were similar to those in the SHAM group (Fig. 6A-6D).

To determine whether the EVs protective effects were associated with anti-oxidative stress regulation, we analyzed the translocation and activation of nuclear factor erythroid 2-related factor 2 (Nrf2) in the nuclei of renal cells (Fig. 6E-6H, 6M). Immunohistochemistry indicated a significant increase in the number of nuclear Nrf2-positive tubule cells in the IRI group (0.27 ± 0.01) compared to SHAM controls (0.1 ± 0.01) (Fig. 6M). Treatment with
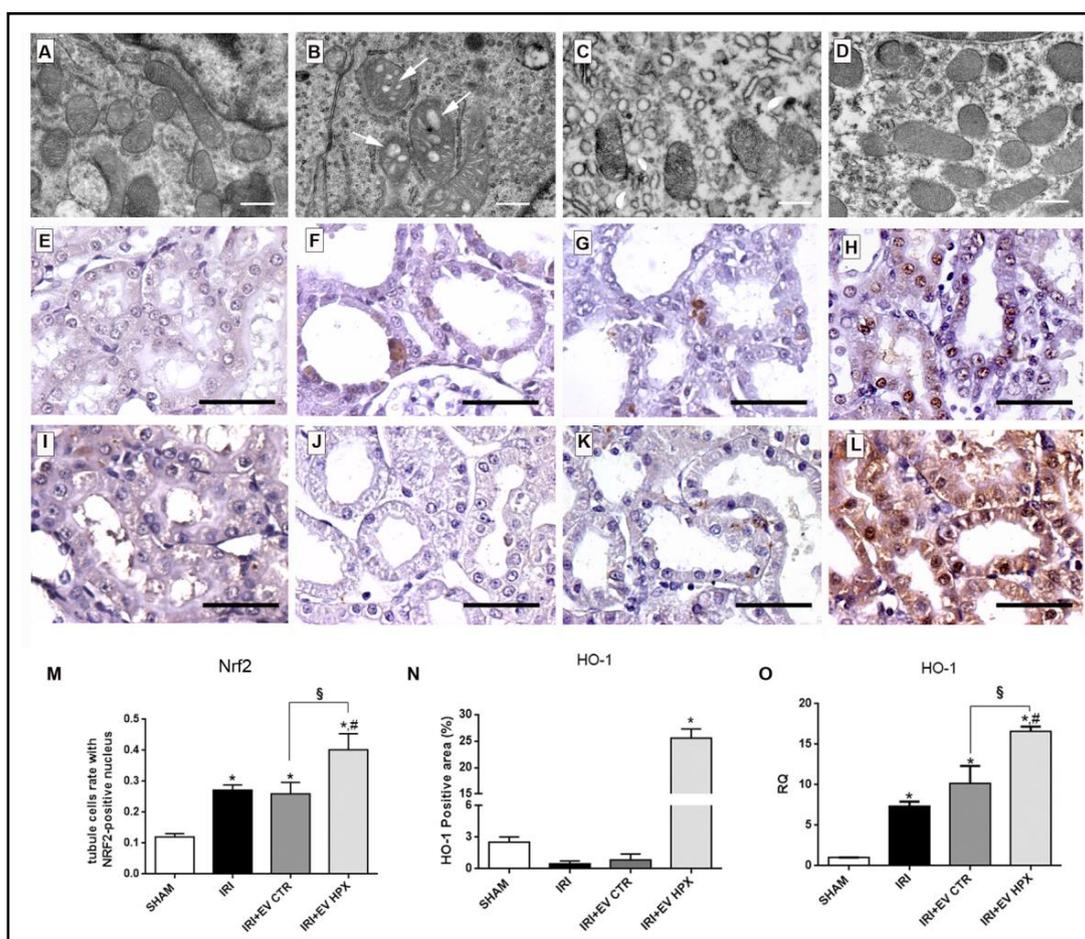
Fig. 6. Mitochondria protection and anti-oxidative stress response in renal cortex tissue modulated by EV CTR and EV HPX. Representative electron microscopy images of mitochondria in the cortical region of the kidney in the different groups: SHAM (A), IRI (B), IRI+EV CTR (C) and IRI+EV HPX (D), (white arrows indicate vacuoles structures, scale bars = 500 nm). Representative photomicrographs of the renal tissue slide immunohistochemistry for Nrf2 in all experimental conditions: SHAM (E), IRI (F), IRI+EV CTR (G), IRI+EV HPX (H), (scale bars = 50 μm). Representative photomicrographs of the renal tissue slide immunohistochemistry for HO-1 in all experimental conditions: SHAM (I), IRI (J), IRI+EV CTR (K), IRI+EV HPX (L), (scale bars = 50 μm). Quantification of the number of tubule cells with nuclear positivity for Nrf2 in relation to the total number of tubule cells/field from immunohistochemistry photomicrographs (n = 6) (M). Quantification of the percentage of area positively marked for HO-1 in each field from immunohistochemistry photomicrographs (n = 6) (N). mRNA levels of HO-1 in renal tissue, expressed as RQ in respect to the SHAM group (n = 5) (O). Data represent mean ± SEM. (* indicates statistical difference to SHAM group; # indicates statistical difference to IRI group, § indicates statistical difference to IRI+EV CTR group, P<0.05 assessed by one-way ANOVA followed by Tukey's test). Abbreviations: EV extracellular vesicles; SHAM, false operate; CTR, control; HPX, hypoxia; IRI, ischemia-reperfusion injury; NFR2, Nuclear factor (erythroid-derived 2)-like 2; HO-1, heme oxygenase 1; RQ, relative quantification.

EV CTR resulted in the same number of Nrf2-positive cells (0.26 ± 0.01) as in the IRI group, whereas the presence of EV HPX strongly increased the number of cells positive for Nrf2 (0.40 ± 0.02) (Fig. 6M). Moreover, immunohistochemical analyses (Fig. 6I-6L, 6N) showed a significant increase in HO-1 protein levels only when EV HPX were given after ischemia (25.6 ± 0.3%). No statistical increase in HO-1 protein levels occurred after EV CTR treatment (0.8 ± 0.3%) compared with untreated IRI (0.5 ± 0.2%, P = 0.98) or SHAM controls (2.5 ± 0.3%, P = 0.38) groups (Fig. 6N). qRT-PCR analyses (Fig. 6O) confirmed the immunohistochemistry

Cellular Physiology and Biochemistry

Cell Physiol Biochem 2019;52:1463-1483

DOI: 10.33594/000000102
Published online: 18 May 2019

© 2019 The Author(s). Published by
Cell Physiol Biochem Press GmbH&Co. KG

1476

Collino et al.: Hypoxia Alters ADMSC-EVs Renoprotective Effects

data, significantly increasing HO-1 expression in EV HPX treated rats with respect to the other conditions. Although EV CTR treatment also increased HO-1 mRNA expression compared to the SHAM group (10-fold increase), this was not statistically different compared to the IRI group (P = 0.3).

Immunomodulatory capacity of EV CTR and EV HPX in promoting renal recovery after IRI
Macrophage infiltration after IRI was assessed immunohistochemically for ED-1 (Fig. 7). The number of macrophages (ED-1 positive cells) increased in the IRI group (9.70 ± 0.43 cells/field) compared with the SHAM group (1.9 ± 0.5 cells/field) (Fig. 7A, 7B, 7E). EV CTR significantly reduced macrophage infiltration (5.0 ± 0.1 cells/field) in the cortical region of the kidney (Fig. 7C, 7E). The effects of EV HPX administration were even more efficient in reducing ED-1 macrophage infiltration, which was similar to that in the SHAM control (2.8 ± 0.1 cells/field) (Fig. 7D, 7E). We also investigated the expression of the inducible nitric oxide synthase (iNOS), a key enzyme in the inflammatory response acting through the release of nitric oxide (NO), and a biomarker for M1-polarized macrophages [30]. qRT-PCR analysis showed a huge upregulation of iNOS under IRI conditions (29-fold increase with respect to the SHAM group), and that the treatment with EV CTR or EV HPX completely reversed iNOS
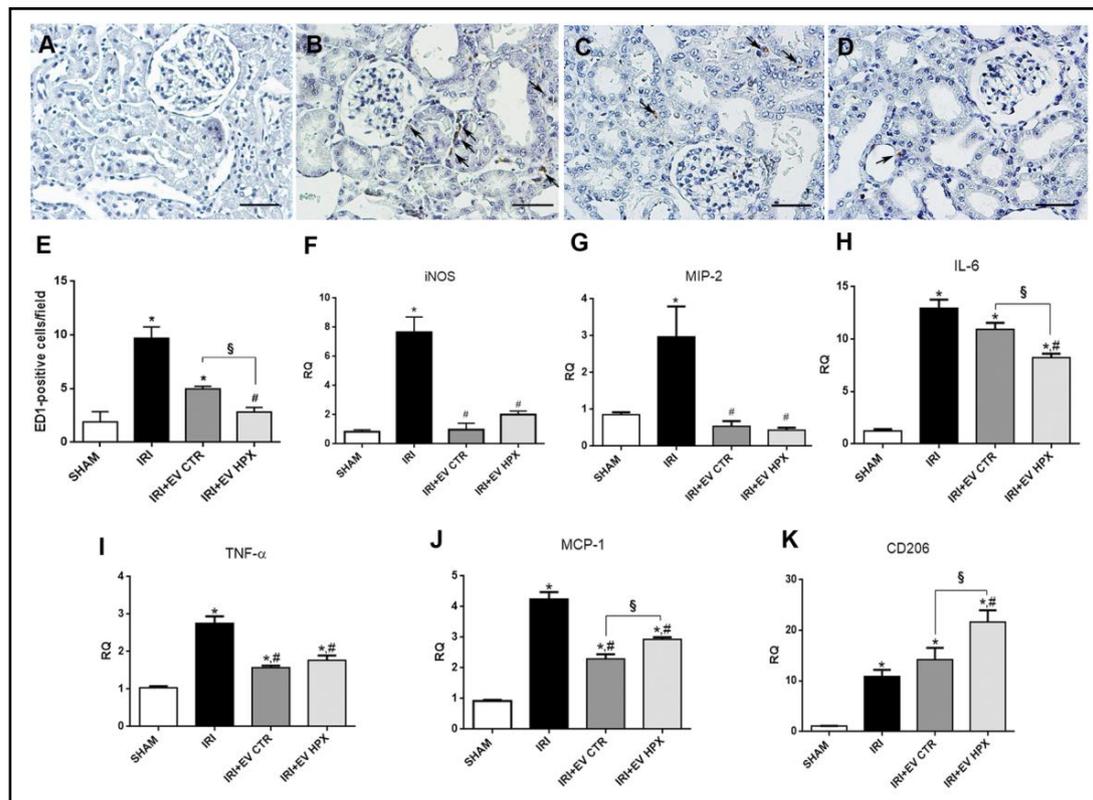

Fig. 7. Immunomodulatory response regulated by EV CTR and EV HPX after kidney injury. Representative photomicrographs of the renal tissue slide immunohistochemistry for ED-1 of the different conditions: SHAM (A), IRI (B), IRI+EV CTR (C) and IRI+EV HPX (D) (scale bars = 50 μm). Quantification of the number of ED-1-positive cells/field (black arrows) from immunohistochemistry photomicrographs (n = 6) (E). mRNA levels of iNOS (F), MIP-2 (G), IL-6 (H), TNF-α (I), MCP-1 (J), CD206 (K) in renal tissue expressed as RQ in respect to SHAM group (n = 5). Data represent mean ± SEM. (* indicates statistical difference to SHAM group; # indicates statistical difference to IRI group, § indicates statistical difference to IRI+EV CTR group, P<0.05 assessed by one-way ANOVA followed by Tukey's test). Abbreviations: EV extracellular vesicles; SHAM, false operate; CTR, control; HPX, hypoxia; IRI, ischemia-reperfusion injury; iNOS, inducible nitric oxide synthase; MIP-2, macrophage inflammatory protein 2; IL, interleukin; TNF-α, tumor necrosis factor-α; MCP-1, monocyte chemoattractant protein-1; RQ, relative quantification.

Cellular Physiology and Biochemistry

Cell Physiol Biochem 2019;52:1463-1483

DOI: 10.33594/000000102
Published online: 18 May 2019

© 2019 The Author(s). Published by
Cell Physiol Biochem Press GmbH&Co. KG

1477

Collino et al.: Hypoxia Alters ADMSC-EVs Renoprotective Effects

mRNA levels to those in the SHAM controls (Fig. 7F). These results show that both types of EVs reduce NO production and, consequently the inflammatory response.

Furthermore, both EVs promoted a completely re-establishment of MIP-2 levels, elevated after IRI (3-fold increase with respect to the level in the SHAM group) (Fig. 7G). IRI animals also showed a strong induction of interleukin (IL)-6 (12-fold increase) with respect to the SHAM animals, and treatment with EV CTR were incapable of reverting this altered pattern (Fig. 7H); on the contrary, EV HPX led to a partial, but significant, downregulation of the raised IL-6 levels induced by IRI.

TNF-α was also upregulated after IRI (3-fold increase with respect to the SHAM group), and administration of EV CTR or EV HPX significantly downregulated its expression in respect to the IRI group (Fig. 7I). Both IL-6 and TNF-α levels after these treatments, though still higher than those in SHAM, showed significant EVs-mediated anti-inflammatory activity. Finally, IRI increased MCP-1 mRNA levels (4-fold change with respect to the SHAM group), which was significantly reduced by the presence of EV CTR compared with the IRI group. This effect was significantly stronger than that with EV HPX, which also promoted a significant downregulation of MCP-1 in comparison with the IRI group (Fig. 7J).

In this immunomodulatory scenario, we determined whether infiltrated macrophages in the kidney were more polarized towards the M2 rather than the M1 phenotype, thus supporting tissue recovery rather than a stimulus to a pro-inflammatory response. The macrophage mannose receptor (CD206) was upregulated by IRI (10-fold increase with respect to SHAM); treatment with EV CTR did not significantly alter this expression (Fig. 7K). The presence of EV HPX during reperfusion, however, resulted in a stronger increase in CD206 expression with respect to both IRI and EV CTR conditions.

Discussion

The properties of EVs are associated with the molecules they carry. Changes in the surrounding environment can alter the secretory pattern of MSCs and specifically the secretion of EVs [31, 32]. We have herein demonstrated that hypoxia can stimulate the secretion of EVs by human ADMSCs, and that these EVs have maintained the renoprotective properties found in EVs derived from ADMSCs under normoxia, decreasing the rate of cell death rate, reducing tissue damage and maintaining adequate kidney functioning. Although both EVs beneficial effects, EV HPX are more potent in mediating renal regeneration. Proteomic analysis on renal cells co-cultured with these vesicles confirmed that they trigger different pathways and processes, indicating that EV HPX present distinctly therapeutic properties of EV CTR.

Adipose tissue is an important and abundant source of MSCs. The regenerative potential of ADMSCs was enhanced by hypoxic conditions that stimulate the secretion of growth factors and cytokines [19]. Our data shows that hypoxia can also stimulate secretion of EVs by ADMSCs without alteration in size distribution or MSC surface markers. We further demonstrated that kidney subcapsular administration delivers EVs to the injured intrarrenal target site, avoiding big losses and maintaining a significant amount of EVs still detectable 24 h after administration. RPTECs were shown to incorporate MSC-EVs [33-35], a process that increases after hypoxic injury provoked by antimycin A [24]. In our model, renal proximal epithelial cells incorporate both EVs similarly, indicating that selective effects result from the molecules they carry.

RPTECs are susceptible to ischemic insult since they have reduced glycolytic capacity and depend on mitochondrial metabolism for ATP synthesis [36]. Since EVs-induced decrease of cell death is the mirror image of EVs-stimulated recovery of intracellular ATP, both beneficial processes may be associated with maintenance of mitochondria structure and energy supply. Interestingly, MSC-EVs express functional respiratory complexes (I, IV, V) and have a respiratory ability independent of whole mitochondria [37]. Therefore, one of the mechanisms associated with the increased renoprotective effects of EV HPX could be

the transfer of components that help to protect mitochondrial and the energy supply in renal cells. Ultimately, EV HPX presented the capability to regulate this process that culminates in the re-establishment of intracellular ATP levels and inhibition of the intrinsic cell death pathway.

Proteomic analysis of RPTECs after injury showed that, in common, both EVs modulate a group of proteins associated to renal recovery (Supplementary Tables 3 and 4). Incubation of RPTECs with EV CTR or EV HPX promoted the downregulation of calnexin, a chaperone protein that interacts with Nox4, a member of the NADPH oxidases family, which is constitutively active in generating H_2O_2 [38]. Downregulation of calnexin promotes disruption of maturation, processing and function of Nox4, resulting in reduced ROS generation [39]. Furthermore, epigenetic regulation was also a common process triggered by both EVs. Expression of histone H2 and histone H2B were upregulated during injury, and EVs treatment abrogated this change. Upregulation of histone is associated with chromatin condensation, a major morphological characteristic of apoptotic cells. In addition, ATP depletion induces chromatin hyper-condensation, reducing transcription activity in cells under a low energy supply [40]. The re-establishment of ATP levels after EVs treatment in RPTECs may be associated with this reversion in histone expression. By analyzing the group of proteins commonly regulated by both EVs, we also saw modulation of other important processes associated with renal recovery, e.g. transcription and translation regulation, cytoskeleton reorganization and protein folding. Some of these processes were also modulated in renal cells by the paracrine actions of BM-MSCs [41], supporting the importance of EVs secretion in the interaction between MSCs and renal cells.

Interestingly, EV CTR and EV HPX also have specific signatures by modulating exclusive groups of proteins. As an example of protein upregulation promoted by EV CTR (Supplementary Table 3), mitogen-activated protein kinase kinase kinase 9 (MAP3K9) deserves special mention as a serine/threonine kinase that phosphorylates MKK7 and MKK4, leading to activation of the JNK pathway, thereby favoring cell proliferation and survival [42]. The group of proteins exclusive of EV CTR is also associated with mitosis and BMP/GDF signal transduction that regulates cell differentiation, proliferation, survival and motility [43]. Finally, we only observed downregulation of fibroblast growth factor receptor 1 (FGFR1) in the presence of EV HPX (Supplementary Table 4). This receptor mediates the epithelial-to-mesenchymal transition induced by TGF-β1 and promotes maladaptive kidney repair in response to injury, inducing renal fibrogenesis [44]. Thus, downregulation of FGFR1 by EV HPX could favor halting of the progressive way from AKI to CKD.

IRI is a complex pathophysiological process characterized by changes in hemodynamic, oxidative stress, inflammation and cell death [45]. IRI drastically reduces blood pressure. Despite the release from renal artery occlusion that results in renal blood flow re-establishment within minutes, a decline of renal blood flow occurs over several hours [46]. As a consequence, damage of endothelial cells and persistent rarefaction of blood vessels, including peritubular capillaries, may interfere in O_2 delivery and waste product removal, inducing fibrotic responses at the final stage [47]. Hypoxia enhances ADMSCs angiogenic stimulatory capacity, as well as that of their secreted EVs [48, 49]. In our study, both EVs possessed angiogenic properties; with a higher angiogenic effect mediated by EV HPX. Such results indicate that EVs, in special EV HPX, can improve the maintenance of renal microvasculature during IRI, preventing fibrosis and impairing to CKD progression.

The beneficial effect of EVs on renal structure and function is through improvement of renal injury score, and by the partial recovery of blood levels of BUN and creatinine – two well known indicators of the renal hemodynamic status – and especially by the downregulation of KIM-1, the specific and sensitive biomarker of acute RPTEC injury [29]. Decreased expression of KIM-1 suggests that EVs act by accelerating phagocytic removal of debris left by dead cells and epithelial recovery [50]. Differently from *in vivo* experiments, both EVs resulted in a better outcome which may be associated with EVs beneficial effects not directly acting on RPTEC cells. However, EV HPX presented a specific feature of cell death inhibition, a proposal that encounters molecular counterpart in the complete re-establishment of Bcl-2/

Cellular Physiology and Biochemistry

Cell Physiol Biochem 2019;52:1463-1483

DOI: 10.33594/000000102
Published online: 18 May 2019

© 2019 The Author(s). Published by
Cell Physiol Biochem Press GmbH&Co. KG

1479

Collino et al.: Hypoxia Alters ADMSC-EVs Renoprotective Effects

Bax levels, which indicate a more protective effect in the regulation of apoptosis. As the Bcl-2 family-related apoptotic process is associated with the loss of integrity of mitochondrial membranes, electron microscopy images of the kidney cortical region showing reversal of the matrix vacuolization found in IRI confirm the efficacy of EVs treatment in terms of oxidative metabolism at the organelle level.

Oxidative stress is an important aspect in the physiopathology of AKI. Nrf2 is an inducible transcription factor that protects renal tissue from IRI damage by regulating multiple cellular antioxidant systems [51]. Once activated, Nrf2 is translocated into the nucleus where it induces the expression of antioxidant genes like HO-1 [51]. Immunohistochemistry analyses showed an increase after IRI in the number of cells with Nfr2 translocated into the nucleus, indicative of an intrinsic response of renal tissue to the oxidative stress. Treatment with EV HPX, but not EV CTR, enhanced Nrf2 translocation and its activation by phosphorylation. As a consequence, there is increased expression of HO-1, a key regulator of processes such as inflammation, apoptosis, oxidative stress, fibrosis, and angiogenesis [52].

Immunomodulatory properties have also been attributed to ADMSC-EVs [53], which also appear to be important in IRI, as shown in the present study. Both EVs could reduce inflammatory response by downregulating pro-inflammatory molecules like iNOS, TNF-α and other molecules associated with macrophage and neutrophil infiltration (MCP-1 and MIP-2). Although the modulation of these key genes was similar with EV CTR and EV HPX, the latter were more effective in reducing IL-6 a major regulator of inflammation. EVs-induced IL-6 downregulation is possibly indicative of protection of RPTECs, since they produce and secrete IL-6 when damaged by local or systemic injury [54]. Moreover, EV HPX downregulation of local IL-6 transcript may also be associated with the reduction in macrophage invasion. Stimulated macrophages produce IL-6 in response to molecules released from damaged RPTECs under IRI, resulting in a maladaptive response [55]. Again, EV HPX were more efficient in reducing macrophage invasion after IRI compared to EV CTR, as demonstrated by the pronounced decrease in the number of ED1-positive cells. Concomitantly, EV HPX increased CD206 expression, which is associated with the presence of M2 macrophage [56, 57]. M2 macrophages have positive regulatory functions in renal tissue repair and remodelling [58], indicating that part of the immunomodulatory properties of EV HPX is associated with macrophage polarization towards M2 phenotype.

Conclusion

We have shown that reduction of pO_2 increases EVs secretion by ADMSCs and enhances some aspects of their renoprotective properties. The differences in the responses to EV CTR and EV HPX indicate that hypoxia promotes changes in the composition of bioactive molecules within the EVs. These changes result in improved outcomes for EV HPX associated with inhibition of apoptosis, immunomodulation, intracellular ATP recovery, angiogenesis, reduction of ROS and preservation of mitochondria, all indicating that hypoxia may be an important tool in promoting the production of ADMSC-EVs for the treatment of kidney diseases. The proteome signatures for the effects of both EVs types indicate the modulation of different cellular process, thus opening vistas to the combination of normoxic and hypoxic EVs for the promotion of more effective beneficial responses.

Acknowledgements

Cellular Physiology and Biochemistry

Cell Physiol Biochem 2019;52:1463-1483

DOI: 10.33594/000000102
Published online: 18 May 2019

© 2019 The Author(s). Published by
Cell Physiol Biochem Press GmbH&Co. KG

1480

Collino et al.: Hypoxia Alters ADMSC-EVs Renoprotective Effects

Disclosure Statement

The authors have no potential conflicts of interest.

References

1   Mehta RL, Cerda J, Burdmann EA, Tonelli M, García-García G, Jha V, Susantitaphong P, Rocco M, Vanholder R, Sever MS, Cruz D, Jaber B, Lameire NH, Lombardi R, Lewington A, Feehally J, Finkelstein F, Levin N, Pannu N, Thomas B, et al.: International Society of Nephrology's 0by25 initiative for acute kidney injury (zero preventable deaths by 2025): a human rights case for nephrology. Lancet 2015;385:2616-2643.

2   Zuk A, Bonventre JV: Acute Kidney Injury. Annu Rev Med 2016;67:293-307.

3   Schrier RW, Wang W, Poole B, Mitra A: Acute renal failure: Definitions, diagnosis, pathogenesis, and therapy. J Clin Invest 2004;114:5-14.

4   Chung AC, Lan HY: Chemokines in renal injury. J Am Soc Nephrol 2011;22:802-809.

5   Lever JM, Boddu R, George JF, Agarwal A: Heme Oxygenase-1 in Kidney Health and Disease. Antioxid Redox Signal 2016;25:165-183.

6   Mattar P, Bieback K: Comparing the immunomodulatory properties of bone marrow, adipose tissue, and birth-associated tissue mesenchymal stromal cells. Front Immunol 2015;6:560-581.

7   Sadat S, Gehmert S, Song YH, Yen Y, Bai X, Gaiser S, Klein H, Alt E: The cardioprotective effect of mesenchymal stem cells is mediated by IGF-I and VEGF. Biochem Biophys Res Commun 2007;363:674-679.

8   Sawada K, Takedachi M, Yamamoto S, Morimoto C, Ozasa M, Iwayama T, Lee CM, Okura H, Matsuyama A, Kitamura M, Murakami S: Trophic factors from adipose tissue-derived multi-lineage progenitor cells promote cytodifferentiation of periodontal ligament cells. Biochem Biophys Res Commun 2015;464:299-305.

9   Rasmussen JG, Frøbert O, Holst-Hansen C, Kastrup J, Baandrup U, Zachar V, Fink T, Simonsen U: Comparison of human adipose-derived stem cells and bone marrow-derived stem cells in a myocardial infarction model. Cell Transplant 2014;23:195-206.

10   Gadelkarim M, Abushouk AI, Ghanem E, Hamaad AM, Saad AM, Abdel-Daim MM: Adipose-derived stem cells: Effectiveness and advances in delivery in diabetic wound healing. Biomed Pharmacother 2018;107:625-633.

11   Tögel F, Zhang P, Hu Z, Westenfelder C: VEGF is a mediator of the renoprotective effects of multipotent marrow stromal cells in acute kidney injury. J Cell Mol Med 2009;13:2109-2114.

12   Lindoso RS, Araujo DS, Adão-Novaes J, Mariante RM, Verdoorn KS, Fragel-Madeira L, Caruso-Neves C, Linden R, Vieyra A, Einicker-Lamas M: Paracrine interaction between bone marrow-derived stem cells and renal epithelial cells. Cell Physiol Biochem 2011;28:267-278.

13   Colombo M, Raposo G, Théry C: Biogenesis, secretion, and intercellular interactions of exosomes and other extracellular vesicles. Annu Rev Cell Dev Biol 2014;30:255-289.

14   Pomatto MAC, Gai C, Bussolati B, Camussi G: Extracellular Vesicles in Renal Pathophysiology. Front Mol Biosci 2017;4:37-58.

15   Zhu F, Chong Lee Shin OLS, Pei G, Hu Z, Yang J, Zhu H, Wang M, Mou J, Sun J, Wang Y, Yang Q, Zhao Z, Xu H, Gao H, Yao W, Luo X, Liao W, Xu G, Zeng R, Yao Y: Adipose-derived mesenchymal stem cells employed exosomes to attenuate AKI-CKD transition through tubular epithelial cell dependent Sox9 activation. Oncotarget 2017;8:70707-70726.

16   Collino F, Pomatto M, Bruno S, Lindoso RS, Tapparo M, Sicheng W, Quesenberry P, Camussi G: Exosome and Microvesicle-Enriched Fractions Isolated from Mesenchymal Stem Cells by Gradient Separation Showed Different Molecular Signatures and Functions on Renal Tubular Epithelial Cells. Stem Cell Rev 2017;13:226-243.

17   Rubina K, Kalinina N, Efimenko A, Lopatina T, Melikhova V, Tsokolaeva Z, Sysoeva V, Tkachuk V, Parfyonova Y: Adipose stromal cells stimulate angiogenesis via promoting progenitor cell differentiation, secretion of angiogenic factors, and enhancing vessel maturation. Tissue Eng Part A 2009;15:2039-2050.

18   Amos PJ, Bailey AM, Shang H, Katz AJ, Lawrence MB, Peirce SM: Functional binding of human adipose-derived stromal cells: effects of extraction method and hypoxia pretreatment. Ann Plast Surg 2008;60:437-444.

19   Zachar V, Duroux M, Emmersen J, Rasmussen JG, Pennisi CP, Yang S, Fink T: Hypoxia and adipose-derived stem cell-based tissue regeneration and engineering. Expert Opin Biol Ther 2011;11:775-786.

20   Lo Sicco C, Reverberi D, Balbi C, Ulivi V, Principi E, Pascucci L, Becherini P, Bosco MC, Varesio L, Franzin C, Pozzobon M, Cancedda R, Tasso R: Mesenchymal Stem Cell-Derived Extracellular Vesicles as Mediators of Anti-Inflammatory Effects: Endorsement of Macrophage Polarization. Stem Cells Transl Med 2017;6:1018-1028.

21   Wilcox AA, Carroll WE, Sterling RE, Davis HA, Ware AG: Use of the Berthelot reaction in the automated analysis of serum urea nitrogen. Clin Chem 1966;12:151-157.

22   Slot C: Plasma creatinine determination. A new and specific Jaffe reaction method. Scand J Clin Lab Invest 1965;17:381-387.

23   Beiral HJ, Rodrigues-Ferreira C, Fernandes AM, Gonsalez SR, Mortari NC, Takiya CM, Sorenson MM, Figueiredo-Freitas C, Galina A, Vieyra A: The impact of stem cells on electron fluxes, proton translocation, and ATP synthesis in kidney mitochondria after ischemia/reperfusion. Cell Transplant 2014;23:207-220.

24   Lindoso RS, Collino F, Bruno S, Araujo DS, Sant'Anna JF, Tetta C, Provero P, Quesenberry PJ, Vieyra A, Einicker-Lamas M, Camussi G: Extracellular vesicles released from mesenchymal stromal cells modulate miRNA in renal tubular cells and inhibit ATP depletion injury. Stem Cells Dev 2014;23:1809-1819.

25   Grange C, Tapparo M, Bruno S, Chatterjee D, Quesenberry PJ, Tetta C, Camussi G: Biodistribution of mesenchymal stem cell-derived extracellular vesicles in a model of acute kidney injury monitored by optical imaging. Int J Mol Med 2014;33:1055-1063.

26   Lindoso RS, Collino F, Camussi G: Extracellular vesicles derived from renal cancer stem cells induce a pro-tumorigenic phenotype in mesenchymal stromal cells. Oncotarget 2015;6:7959-7969.

27   Mbeunkui F, Goshe MB: Investigation of solubilization and digestion methods for microsomal membrane proteome analysis using data-independent LC-MSE. Proteomics 2011;11:898-911.

28   Corrêa S, Panis C, Binato R, Herrera AC, Pizzatti L, Abdelhay E: Identifying potential markers in Breast Cancer subtypes using plasma label-free proteomics. J Proteomics 2017;151:33-42.

29   Bonventre JV: Kidney Injury Molecule-1 (KIM-1): a specific and sensitive biomarker of kidney injury. Scand J Clin Lab Invest Suppl 2008;241:78-83.

30   Jablonski KA, Amici SA, Webb LM, Ruiz-Rosado Jde D, Popovich PG, Partida-Sanchez S, Guerau-de-Arellano M: Novel Markers to Delineate Murine M1 and M2 Macrophages. PLoS One 2015;10:e0145342.

31   Madrigal M, Rao KS, Riordan NH: A review of therapeutic effects of mesenchymal stem cell secretions and induction of secretory modification by different culture methods. J Transl Med 2014;12:260.

32   Kusuma GD, Carthew J, Lim R, Frith JE: Effect of the Microenvironment on Mesenchymal Stem Cell Paracrine Signaling: Opportunities to Engineer the Therapeutic Effect. Stem Cells Dev 2017;26:617-631.

Cellular Physiology and Biochemistry

Cell Physiol Biochem 2019;52:1463-1483

DOI: 10.33594/000000102
Published online: 18 May 2019

© 2019 The Author(s). Published by
Cell Physiol Biochem Press GmbH&Co. KG

1482

Collino et al.: Hypoxia Alters ADMSC-EVs Renoprotective Effects

33   Eirin A, Zhu XY, Puranik AS, Tang H, McGurren KA, van Wijnen AJ, Lerman A, Lerman LO: Mesenchymal stem cell-derived extracellular vesicles attenuate kidney inflammation. Kidney Int 2017;92:114-124.

34   Choi HY, Moon SJ, Ratliff BB, Ahn SH, Jung A, Lee M, Lee S, Lim BJ, Kim BS, Plotkin MD, Ha SK, Park HC: Microparticles from kidney-derived mesenchymal stem cells act as carriers of proangiogenic signals and contribute to recovery from acute kidney injury. PLoS One 2014;9:e87853.

35   Choi HY, Lee HG, Kim BS, Ahn SH, Jung A, Lee M, Lee JE, Kim HJ, Ha SK, Park HC: Mesenchymal stem cell-derived microparticles ameliorate peritubular capillary rarefaction via inhibition of endothelial-mesenchymal transition and decrease tubulointerstitial fibrosis in unilateral ureteral obstruction. Stem Cell Res Ther 2015;6:18.

36   Uchida S, Endou H: Substrate specificity to maintain cellular ATP along the mouse nephron. Am J Physiol 1988;255:F977-F983.

37   Panfoli I, Ravera S, Podestà M, Cossu C, Santucci L, Bartolucci M, Bruschi M, Calzia D, Sabatini F, Bruschettini M, Ramenghi LA, Romantsik O, Marimpietri D, Pistoia V, Ghiggeri G, Frassoni F, Candiano G: Exosomes from human mesenchymal stem cells conduct aerobic metabolism in term and preterm newborn infants. FASEB J 2016;30:1416-1424.

38   Brandes RP, Weissmann N, Schröder K: Nox family NADPH oxidases: Molecular mechanisms of activation. Free Radic Biol Med 2014;76:208-226.

39   Prior KK, Wittig I, Leisegang MS, Groenendyk J, Weissmann N, Michalak M, Jansen-Dürr P, Shah AM, Brandes RP: The Endoplasmic Reticulum Chaperone Calnexin is a NADPH Oxidase NOX4 Interacting Protein. J Biol Chem 2016;291:7045-7059.

40   Visvanathan A, Ahmed K, Even-Faitelson L: Modulation of Higher Order Chromatin Conformation in Mammalian Cell Nuclei Can Be Mediated by Polyamines and Divalent Cations. PLoS One 2013;8:e67689.

41   da Costa MR, Pizzatti L, Lindoso RS, Sant'Anna JF, DuRocher B, Abdelhay E, Vieyra A: Mechanisms of kidney repair by human mesenchymal stromal cells after ischemia: a comprehensive view using label-free MS(E). Proteomics 2014;14:1480-1493.

42   Wagner EF, Nebreda AR: Signal integration by JNK and p38 MAPK pathways in cancer development. Nat Rev Cancer 2009;9:537-549.

43   Vigolo E, Markó L, Hinze C, Müller DN, Schmidt-Ullrich R, Schmidt-Ott KM: Canonical BMP signaling in tubular cells mediates recovery after acute kidney injury. Kidney Int 2018;95:108-122.

44   Lovisa S, LeBleu VS, Tampe B, Sugimoto H, Vadnagara K, Carstens JL, Wu CC, Hagos Y, Burckhardt BC, Pentcheva-Hoang T, Nischal H, Allison JP, Zeisberg M, Kalluri R: Epithelial-to mesenchymal transition induces cell cycle arrest and parenchymal damage in renal fibrosis. Nat Med 2015;21:998-1009.

45   Basile DP, Anderson MD, Sutton TA: Pathophysiology of acute kidney injury. Compr Physiol 2012;2:1303-1353.

46   Cristol JP, Thiemermann C, Mitchell JA, Walder C, Vane JR: Support of renal blood flow after ischaemic-reperfusion injury by endogenous formation of nitric oxide and of cyclo-oxygenase vasodilator metabolites. Br J Pharmacol 1993;109:188-194.

47   Basile DP: The endothelial cell in ischemic acute kidney injury: implications for acute and chronic function. Kidney Int 2007;72:151-156.

48   Han Y, Ren J, Bai Y, Pei X, Han Y: Exosomes from hypoxia-treated human adipose-derived mesenchymal stem cells enhance angiogenesis through VEGF/VEGF-R. Int J Biochem Cell Biol 2019;109:59-68.

49   Xue C, Shen Y, Li X, Li B, Zhao S, Gu J, Chen Y, Ma B, Wei J, Han Q, Zhao RC: Exosomes Derived from Hypoxia-Treated Human Adipose Mesenchymal Stem Cells Enhance Angiogenesis Through the PKA Signaling Pathway. Stem Cells Dev 2018;27:456-465.

50   Ichimura T, Asseldonk EJ, Humphreys BD, Gunaratnam L, Duffield JS, Bonventre JV: Kidney injury molecule-1 is a phosphatidylserine receptor that confers a phagocytic phenotype on epithelial cells. J Clin Invest 2008;118:1657-1668.

51   Shokeir AA, Hussein AM, Barakat N, Abdelaziz A, Elgarba M, Awadalla A: Activation of nuclear factor erythroid 2-related factor 2 (Nrf2) and Nrf-2-dependent genes by ischemic pre-conditioning and post-conditioning: new adaptive endogenous protective responses against renal ischaemia/reperfusion injury. Acta Physiol (Oxf) 2014;210:342-353.

52   Loboda A, Damulewicz M, Pyza E, Jozkowicz A, Dulak J: Role of Nrf2/HO-1 system in development, oxidative stress response and diseases: an evolutionarily conserved mechanism. Cell Mol Life Sci 2016;73:3221-3247.

53   Roemeling-van Rhijn M, Mensah FK, Korevaar SS, Leijs MJ, van Osch GJ, Ijzermans JN, Betjes MG, Baan CC, Weimar W, Hoogduijn MJ: Effects of Hypoxia on the Immunomodulatory Properties of Adipose Tissue-Derived Mesenchymal Stem cells. Front Immunol 2013;4:203.

54   Su H, Lei CT, Zhang C: Interleukin-6 Signaling Pathway and Its Role in Kidney Disease: An Update. Front Immunol 2017;8:405.

55   Kielar ML, John R, Bennett M, Richardson JA, Shelton JM, Chen L, Jeyarajah DR, Zhou XJ, Zhou H, Chiquett B, Nagami GT, Lu CY: Maladaptive role of IL-6 in ischemic acute renal failure. J Am Soc Nephrol 2005;16:3315-3325.

56   Stout RD, Jiang C, Matta B, Tietzel I, Watkins SK, Suttles J: Macrophages sequentially change their functional phenotype in response to changes in microenvironmental influences. J Immunol 2005;175:342-349.

57   Li J, Liu CH, Xu DL, Gao B: Clinicopathological significance of CD206-positive macrophages in patients with acute tubulointerstitial disease. Int J Clin Exp Pathol 2015;8:11386-11392.

58   Meng XM, Tang PM, Li J, Lan HY: Macrophage Phenotype in Kidney Injury and Repair. Kidney Dis (Basel) 2015;1:138-146.